5th International Conference on Experimental Fluid Mechanics – ICEFM 2018 Munich
Munich, Germany, July 2-4, 2018

Scale interaction in a turbulent boundary layer perturbed by a cylindrical element

Zhanqi Tang[1]*, Nan Jiang[2#]

[1] Department of Mechanics, Tianjin University, Tianjin 300350, China

[2] Tianjin Key Laboratory of Modern Engineering Mechanics, Tianjin 300350, China

* zhanqitang@tju.edu.cn

nanj@tju.edu.cn

Abstract

The modifications of scale interaction in a turbulent boundary layer perturbed by a wall-mounted circular cylinder were observed, by hot-wire measurements executed downstream of the cylindrical element. The streamwise fluctuating signals were decomposed into large-, small- and dissipative-scale signatures by corresponding cutoff filters. The scale interaction under the cylindrical perturbation were elaborated, by comparing the small- and dissipative-scale amplitude/frequency modulation effects downstream of the cylinder element with the results observed in unperturbed case. It was obtained that the large-scale fluctuations perform a stronger amplitude modulation on both the small and dissipative scales in the near-wall region. At the wall-normal positions of the cylinder height, the small-scale amplitude modulation coefficients are redistributed by cylinder wake. The similar observation was noted in small-scale frequency modulation, however, the dissipative-scale frequency modulation seems to be independent of the cylindrical perturbation. The phase-relationship observation indicated that the cylindrical perturbation shortens the time shifts between both the small- and dissipative-scale variations (amplitude and frequency) and large-scale fluctuations.

1 Introduction

Advances in particle image velocimetry (PIV) and direct numerical simulation (DNS), most researchers have paid more attentions to the outer layer region of turbulent boundary layer flows where the large-scale scale structures dominate, rather than the near-wall region. The large-scale structures are characterized as uniform momentum zones (UMZs) by presenting relatively coherent streamwise velocity, which are demarcated by thin shear interfaces clustered by a large proportion of vorticity (Adrian et al. 2000). A conceptual framework to combine the UMZs and high shear regions was proposed as hairpin vortex packets developed by Adrian et al. (Adrian, et al. 2000). Furthermore, the streamwise-stretched low- and high-speed regions alternatively occur in the spanwise direction, and the low-speed regions were explained as the zones between the legs of aligned packets of hairpin vortices (Tomkins and Adrian 2003). The low-speed regions extend several boundary layer thicknesses in the streamwise direction, and the formation was regarded as the streamwise alignment of hairpin packets (Zhou et al. 1999). To observe these "meandering" large-scale structures, Hutchins and Marusic (Hutchins and Marusic 2007) found that they extend over 20 δ in length (where δ is the boundary layer thickness) in high Reynolds number case, and the energy content of these very large-scale structures (termed as "superstructures") increases with Reynolds number.

More importantly, as these very large-scale structures perform an amplitude modulation on the near-wall cycle, it attracted many studies to quantify the amplitude modulation (AM) effect (Mathis et al. 2009). Even though Schlatter and Örlü (Schlatter and Örlü 2010) demonstrated that AM correlation coefficient may not be an independent tool to quantify the AM effect, they did believe that there exists scale interaction between

large and small scales in turbulent boundary layer flows, and the scale interaction effect has been supported by numerous following studies (Baars et al. 2015, Ganapathisubramani et al. 2012). On the other hand, the observation of frequency modulation (FM) has also been achieved by both discrete technique (Ganapathisubramani, et al. 2012) and continuous analysis (Baars et al. 2017, Baars, et al. 2015). Furthermore, the phase relationship between the large-scale fluctuations and small-scale amplitude/frequency realizations has been investigated (Chung and McKeon 2010). Baars et al. (Baars, et al. 2017, Baars, et al. 2015) further presented a conceptual mechanism of the scale interaction and arrangement in the turbulent boundary layer, which could be described from three regimes. In the near-wall region, a quasi-steady response of the near-wall cycle to large-scale changes in the outer flow was raised, and it was further proved as a "Quasi-Steady, Quasi Homogenous (QSQH)" response (Zhang and Chernyshenko 2016). In the intermittent region, owing to the turbulent/non-turbulent zone intermittency, a reversed scale-interaction phenomenon was observed in contrast to the near-wall region. Moreover, at the centre of the log layer, the conditionally averaging results indicated that the largest fluctuations in the small-scale turbulence are aligned with the internal shear layers along the inclined back of low speed motions.
From the above, it can be seen that the large-scale structures are the key ingredient, and perform as the determinant in the scale interaction and arrangement of the turbulent boundary layer. In other words, altering large-scale structures could offer an opportunity to modify the interaction of the large- and small-scale motions, and probably provide a potential approach to change the near-wall cycle and achieve the drag reduction. In the previous investigations, roughness element has been imposed in the turbulent boundary layer, which were meant to modify the large-scale structures (Pathikonda and Christensen 2014, Tang et al. 2016, Tang et al. 2017, Wang et al. 2018). Following the previous investigations, the current study continues exploring the scales interaction in the turbulent boundary layer flow under the perturbation of a wall-mounted cylindrical element.

2 Experimental set-up

Experiments were conducted in a closed-circuit wind tunnel. The test section of the tunnel was 2.0 m×0.6 m ×0.8 m (length×height×width), and a boundary-layer plate was vertically fastened at the test section. Zero-pressure-gradient conditions were achieved by adjusting the inclination angle of the experimental plate. A trip wire of 2mm height and a 240-grit sandpaper trip band were utilized to accelerate the development of the fully-developed turbulent boundary layer. The freestream velocity was 9.0 m/s, and a turbulent boundary layer was developed with a thickness of 38 mm. The Reynolds number was $\mathrm{Re}_\tau = 980$. Previous study provides a more detailed description of this facility and flow conditions (Tang and Jiang 2018, Tang, et al. 2016).
Hot-wire measurements were carried out in the turbulent boundary layer. A miniature single sensor boundary layer probe (TSI-1621A-T1.5) was used with a constant temperature anemometer system of IFA-300 operating at an overheat ratio of 1.7. The tungsten hot wire has the sensitive length of 1.25 mm (the viscous scaled length of $l^+ = lu_\tau/\nu = 32.6$) and the diameter of 4 μm, corresponding to a length-to-diameter ratio (l/d) more than 200. Calibration was employed by Air Velocity Calibrator over a velocity range of 0 to 18m/s. The hot-wire probe was translated to all the measurement locations by using a computer-controlled translation stage. The sampling frequency and low-pass filter settings were $f = 20$k Hz and $f_{lp} = 10$k Hz, respectively. The non-dimensional sample interval was $\Delta t^+ = 0.51$ ($\Delta t^+ = \Delta t u_\tau^2/\nu$, where$\Delta t = 1/f$), to ensure that the smallest scales were adequately resolved (Hutchins et al. 2009, Mathis, et al. 2009). The sample length of 52.4 seconds of the velocity samples were recorded at each measurement point, which includes 12850 boundary-layer turnover time.
As the benchmark for comparison, unperturbed TBL-flow measurement was performed at the streamwise location of $x = 1.35$m downstream of the leading edge, where the turbulent boundary layer was fully developed. This streamwise location was set as the reference position to mount the cylindrical element. As the experimental sketch shown in Fig. 1, the cylindrical element has a height of $H = 7$mm ($H/\delta = 0.19$, $H^+ = 180$) and a diameter of $d = 12$mm ($d/\delta \approx 0.32$). The present cylindrical element has a low aspect

ratio of AR=0.58. The coordinates x, y and z refer to the streamwise, wall-normal and spanwise directions. Downstream of the cylindrical element, 8 streamwise locations ($x/d = n, n = 3\sim10$) along the center axis of the cylindrical element were measured, starting from $3d$ downstream of the cylindrical element (comfortably downstream of the recirculation zone) to $10d$ within the fixed streamwise spacing of $1d$.

3 Amplitude and Frequency Modulation coefficients

The amplitude and frequency modulation (AM and FM) effects of the large-scale fluctuations on small and dissipative scales are obtained, by computing the cross-correlation coefficients between the large scales and the large-scale variations of the amplitude/frequency time series on the corresponding scales (Tang and Jiang 2018). Fig. 1 shows the evolution of the AM and FM correlation results with zero-time-delay downstream of the cylindrical element perturbation. The left column presents the AM distributions of the small- and dissipative-scale fluctuations ($R_{\mathrm{AM}}(\mathrm{L},\mathrm{S})$ and $R_{\mathrm{AM}}(\mathrm{L},\mathrm{D})$), and the small- and dissipative-scale FM coefficient distributions are plotted in the right column. As shown, all the modulation coefficients are the function of the wall-normal position.

In Fig. 1 (a) and (b), $R_{\mathrm{AM}}(\mathrm{L},\mathrm{S})$ and $R_{\mathrm{AM}}(\mathrm{L},\mathrm{D})$ perform the similar evolution downstream of the cylindrical element. By comparing with the unperturbed case as shown in black line, the cylindrical perturbation exhibits the obvious influence on the AM coefficients in the near-wall region and the region around the top of the log layer. In the near wall region, the AM correlation shows high positive coefficients at the downstream position of $x = 3d$, then it decreases along the sateamwise direction, even lower than the results in the unperturbed case at the end of measurement region. The evolution of the AM coefficients indicates that the modulation extent of the large-scale structures on both the small and dissipative scales, are enhanced at first and then attenuated in the downstream locations. For the region around the top of log layer, AM correlation presents obvious negative coefficients under the perturbation. It indicates that the small scales with relatively higher amplitude occur in the low-speed zones, and vice versa. It probably infers that in the cylinder wake region the relatively high-speed large scales carrying the low-intensity fluids, move from the upper region towards the wall following the downwash flow (Pathikonda and Christensen 2014, Tang, et al. 2016), meanwhile, the low-speed motions with the high-intensity fluctuations in the internal region move upwards. This potential frame is very similar as the intermittency in the wake region, but it arises from the new-generated structures induced by the cylindrical element. In addition, beyond the wall-normal height of $y/\delta > 0.4$, the distribution of both $R_{\mathrm{AM}}(\mathrm{L},\mathrm{S})$ and $R_{\mathrm{AM}}(\mathrm{L},\mathrm{D})$ collapse at all the streamwise locations, which signifies that both the small- and dissipative-scale AM coefficients are independent of the cylindrical element impact in the current experiment.

Fig. 1 (c) and (d) shows the frequency modulation of the large-scale fluctuations on the small and dissipative scales ($R_{\mathrm{FM}}(\mathrm{L},\mathrm{S})$ and $R_{\mathrm{FM}}(\mathrm{L},\mathrm{D})$), respectively. The small- and dissipative-scale FM coefficients have the different distributions under the cylindrical perturbation. In Fig. 1 (c), in the near-wall region, $R_{\mathrm{FM}}(\mathrm{L},\mathrm{S})$ is enhanced, and then gradually decreased along the streamwise direction. At the top region of the log layer, a negative-FM-coefficient trend appears. This negative-coefficient distribution should be also connected to cylinder wake effect as explained in the AM effects (Fig. 1 (a) and (b)). In the wake region of $y/\delta > 0.4$, it can be seen that the cylindrical element does not affect the small-scale FM configuration. Furthermore, Fig. 1 (d) plots the evolution of the dissipative-scale FM. The FM coefficients under the perturbation show the similar distribution as the unperturbed case, but present the relatively lower correlation. This configuration implies that the dissipative-scale frequency modulation is attenuated downstream of the cylindrical element.

Fig. 2 (a) and (b) respectively plot the evolution of the time shift of the small- and dissipative-scale amplitudes relative to the large scales. The time shifts have the similar evolution for the small and dissipative scales. For the time shift of positive coefficients (marked by squares), the time-shift value of both scales (S and D) is decreased under the perturbation. It indicates that the cylindrical perturbation attenuates the temporal lead of the small-/dissipative-scale amplitude relative to the large-scale fluctuations. For the time shift corresponding to the negative coefficients (marked by triangles), it can be seen that in the region of

$y^+ \approx 100\sim300$, the lag is narrowed due to the effect of cylindrical element. The cylinder influence on the lag phase shift lasts to the end of measurement region.
Right column shows the time shifts of the small- and dissipative frequency signature with respect to the large scales, respectively. In Fig. 2 (c), the cylindrical perturbation can be noted in the near-wall region. It reduces the temporal lead of small-scale frequency. For the dissipative-scale frequency in Fig. 2 (d), the time shifts under the perturbation are around $\tau^+ \approx 0$. As convecting downstream, the time-shift distributions gradually get close to be the trend as shown in the unperturbed case.

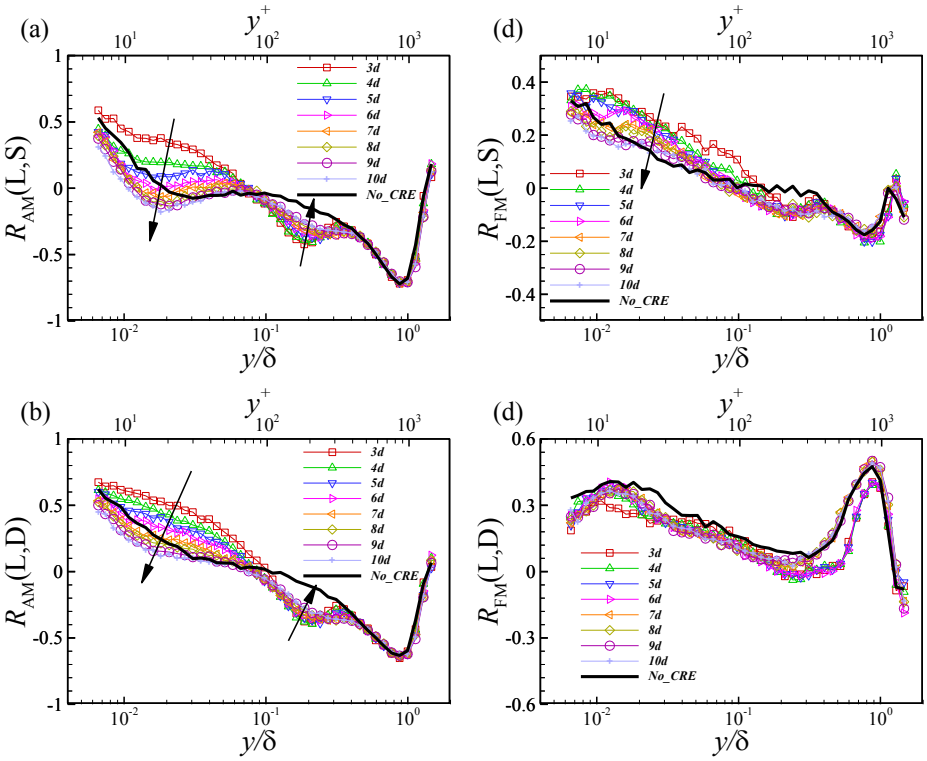

Fig. 1 Evolution of the zero-time-delay amplitude modulation (left column, (a): $R_{AM}(L,S)$, (b): $R_{AM}(L,D)$) and frequency modulation (right column, (c): $R_{FM}(L,S)$, (d): $R_{FM}(L,D)$ at different several streamwise locations ($x = 3\sim10d$) downstream of the cylindrical element. The results of the unperturbed cases are marked by black line for comparison. Note that L, S, D represent large, small, and dissipative sales respectively.

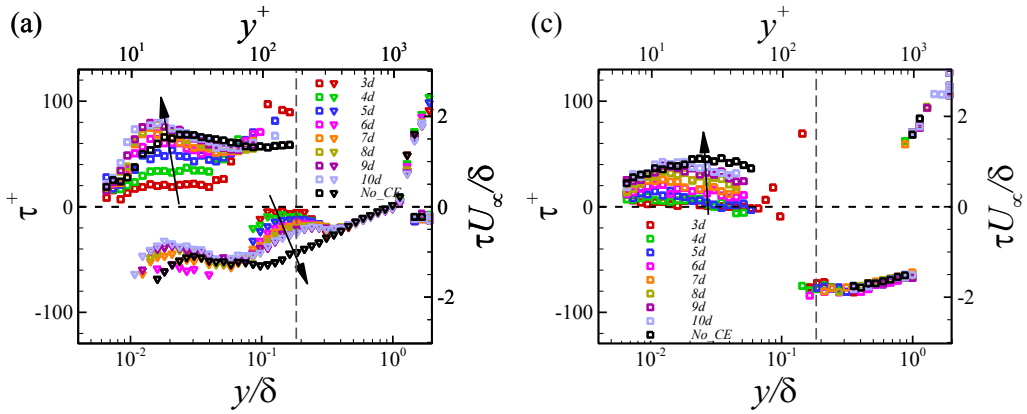

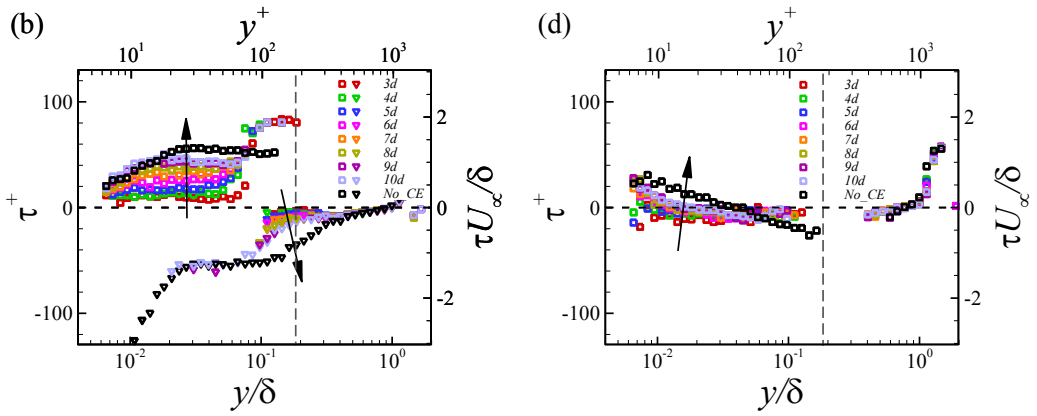

Fig. 2. Evolutions of the phase shifts ($\tau^+; \tau U_\infty/\delta$) of the (a) small-scale amplitude, (b) dissipative-scale amplitude, (c) small-scale frequency and (d) dissipative-scale frequency signature relative to the large-scale fluctuations downstream of the cylindrical perturbation. The results of the unperturbed case are also plotted for comparison.

4 Conclusion

For the amplitude modulation and time shifts, the small and dissipative scales exhibited the similar distribution in the canonical turbulent boundary layer. The similarity was also found under the cylindrical perturbation. Downstream of the cylindrical element, there were three dominant characteristics observed on the AM effect: 1) in the near wall region, large-scale fluctuations perform a stronger AM effect on both small and dissipative scales in the case without time shifts, 2) at the region corresponding to the cylinder height, both S- and D-scale AM coefficients present the lower negative values, by implying a preferential scale arrangement probably caused by the outer/inter fluid exchange in the cylinder wake flow, 3) both the S- and D-scale AM time shifts with respect to the large scales are reduced in the above two regions.

The FM effect of large scales on both small and dissipative scales were observed in the near wall region, by showing the obvious positive FM coefficients. In the wake region, even though the FM coefficients become opposite for the small (negative) and dissipative (positive) scales, the causes of both distributions could be attributed to the turbulent/non-turbulent intermittency. The dissipative scales were speculated to be connected with the background turbulence in the main flow, which are characterized as low intensity but high frequency, so the dissipative scales returned the positive FM coefficients in the intermittent region. As similar as the AM effect, the cylindrical perturbation had an impact on the S-scale FM effect in both the near-wall region and the region corresponding to the cylinder height, however, the dissipative-scale FM seemed to be independent of the cylinder impact. For the FM time shifts, it was found that the phase shifts between the small/dissipative scales and the large scales are shortened in the near-wall region under the perturbation.

Acknowledgements

This work was supported by the National Natural Science Foundation of China with Grant Nos. 11502066, 11332006, 11732010 and 11572221, and the China Postdoctoral Science Foundation.

References

Adrian RJ, et al. (2000) Vortex organization in the outer region of the turbulent boundary layer. *Journal of Fluid Mechanics* 422:1-54

Baars WJ, et al. (2017) Reynolds number trend of hierarchies and scale interactions in turbulent boundary layers. *Philosophical transactions Series A, Mathematical, physical, and engineering sciences* 375

Baars WJ, et al. (2015) Wavelet analysis of wall turbulence to study large-scale modulation of small scales. *Experiments in fluids* 56

Chung D, McKeon BJ (2010) Large-eddy simulation of large-scale structures in long channel flow. *Journal of Fluid Mechanics* 661:341-364

Ganapathisubramani B, et al. (2012) Amplitude and frequency modulation in wall turbulence. *Journal of Fluid Mechanics* 712:61-91

Hutchins N, Marusic I (2007) Evidence of very long meandering features in the logarithmic region of turbulent boundary layers. *Journal of Fluid Mechanics* 579:1-28

Hutchins N, et al. (2009) Hot-wire spatial resolution issues in wall-bounded turbulence. *Journal of Fluid Mechanics* 635:103

Mathis R, et al. (2009) Large-scale amplitude modulation of the small-scale structures in turbulent boundary layers. *Journal of Fluid Mechanics* 628:311

Pathikonda G, Christensen KT (2014) Structure of Turbulent Channel Flow Perturbed by a Wall-Mounted Cylindrical Element. *AIAA Journal*:1-10

Schlatter P, Örlü R (2010) Quantifying the interaction between large and small scales in wall-bounded turbulent flows: A note of caution. *Physics of Fluids* 22:051704

Tang Z, Jiang N (2018) Scale interaction and arrangement in a turbulent boundary layer perturbed by a wall-mounted cylindrical element. *Physics of Fluids* 30

Tang Z, et al. (2016) Bursting process of large- and small-scale structures in turbulent boundary layer perturbed by a cylinder roughness element. *Experiments in fluids* 57

Tang Z, et al. (2017) PIV Measurements of a Turbulent Boundary Layer Perturbed by a Wall-Mounted Transverse Circular Cylinder Element. *Flow, Turbulence and Combustion* 100:365-389

Tomkins CD, Adrian RJ (2003) Spanwise structure and scale growth in turbulent boundary layers. *Journal of Fluid Mechanics* 490:37-74

Wang J, et al. (2018) Modulating the Near-Wall Velocity Fields in Wall-Bounded Turbulence via Discrete Surface Roughness. *AIAA Journal*:1-11

Zhang C, Chernyshenko SI (2016) Quasisteady quasihomogeneous description of the scale interactions in near-wall turbulence. *Physical Review Fluids* 1

Zhou J, et al. (1999) Mechanisms for generating coherent packets of hairpin vortices in channel flow. *Journal of Fluid Mechanics* 387:353-396